Geomagnetic storms over the last solar cycle: A superposed epoch analysis

J. A. Hutchinson,[1] D. M. Wright,[1] and S. E. Milan[1]

Received 11 January 2011; revised 12 May 2011; accepted 27 June 2011; published 13 September 2011.

[1] Presented here is a discussion of the results of a superposed epoch analysis of geomagnetic storms over the last solar cycle. Storms, identified by means of their characteristic *SYM-H* evolution, are separated by size into weak ($-150 < SYM\text{-}H \leq -80$) nT, moderate ($-300 < SYM\text{-}H \leq -150$) nT, and intense ($SYM\text{-}H \leq -300$) nT categories. Where possible, the corresponding solar wind (SW) onset mechanisms were located by means of 1 min ACE OMNI data. Intense storms were observed to be driven solely by coronal mass ejections (CMEs); moderate storms were dominated by CME onset, while only weak storms were driven by both CMEs and corotating interaction regions (CIRs) at a ratio of ~2:1, respectively. As might be expected, more intense storms resulted from the largest SW enhancements. Individual storm phase durations for different storm sizes were investigated, revealing that the duration of the main phase increases with storm size to a critical point, then decreases for more intense storms, contrary to the findings of a previous study by Yokoyama and Kamide (1997). Various SW-magnetosphere coupling functions were investigated for this data set in an attempt to estimate storm size from SW conditions.

Citation: Hutchinson, J. A., D. M. Wright, and S. E. Milan (2011), Geomagnetic storms over the last solar cycle: A superposed epoch analysis, *J. Geophys. Res.*, *116*, A09211, doi:10.1029/2011JA016463.

1. Introduction

[2] Geomagnetic storms are generally defined by periods of intense solar wind–magnetosphere (SW-M) coupling usually associated with extreme conditions in the solar wind (SW), such as coronal mass ejections (CMEs) or co-rotating interaction regions (CIRs). They cause large global disturbances in the Earth's magnetosphere [*Akasofu et al.*, 1963; *Gosling et al.*, 1990; *Gonzalez et al.*, 1994] during which, large amounts of energy are stored in the magnetotail and inner magnetosphere, producing an enhanced ring current and energizing plasma to relativistic levels through not yet fully understood excitation mechanisms [e.g., *Daglis et al.*, 1999, and references therein; *Daglis and Kozyra*, 2002]. Storms have been shown to be a separate phenomenon to substorms [e.g., *Gonzalez et al.*, 1994; *Taylor et al.*, 1994; *Gonzalez et al.*, 1999], and not just a simple superposition of substorm events causing a larger global disturbance and ring current enhancement. While increased and more intense substorm activity is seen during storm periods, the reverse is not true that increased substorm activity has to be a result of storms [e.g., *Gonzalez et al.*, 1994; *Taylor et al.*, 1994; *Gonzalez et al.*, 1999].

[3] Storms can be easily identified from their characteristic *SYM-H* variation (see Figure 1). *SYM-H* is a geomagnetic index giving a measure of the ring current from ground-based equatorial magnetometers showing the deflection of the terrestrial magnetic field caused by the induced, opposing magnetic field from the increased ring current [*Wanliss and Showalter*, 2006].

[4] Generally speaking, storms consist of three phases, an initial, main and recovery phase; each clearly demarked in the *SYM-H* trace above and with different associated SW properties and geomagnetic processes. Increased SW ram pressure, associated with a CME or CIR striking the dayside magnetopause, causes compression of the terrestrial field and increases the field strength resulting in a small positive increase in *SYM-H*.

[5] Main phase commencement, and storm progression in general, is strongly controlled by the Interplanetary Magnetic Field (IMF) B_Z component [e.g., *Echer et al.*, 2008; *Milan et al.*, 2009]. At the onset of favorable IMF conditions, fast dayside reconnection drives the main phase of the storm depositing a large amount of energy, of the order of a few 10^{31} keV, into the magnetosphere [*Kozyra et al.*, 1998]. The ring current is enhanced by some still unknown process. This increase in ring current strength leads to a depression in the terrestrial magnetic field as seen in the sudden drop in *SYM-H* trace in Figure 1. It has been shown that the radius of the auroral oval is closely linked to the size of the ring current enhancement or storm progression, and that this in turn is highly correlated to SW properties and coupling functions such as the dayside reconnection rate [*Milan et al.*, 2009].

[6] The end of the main phase and start of recovery are usually attributed to a reduction in the driving conditions on the dayside, such as reduced SW velocity or a turning of the IMF B_Z to less negative or positive values.

[1]Department of Physics and Astronomy, University of Leicester, Leicester, UK.

0148-0227/11/2011JA016463

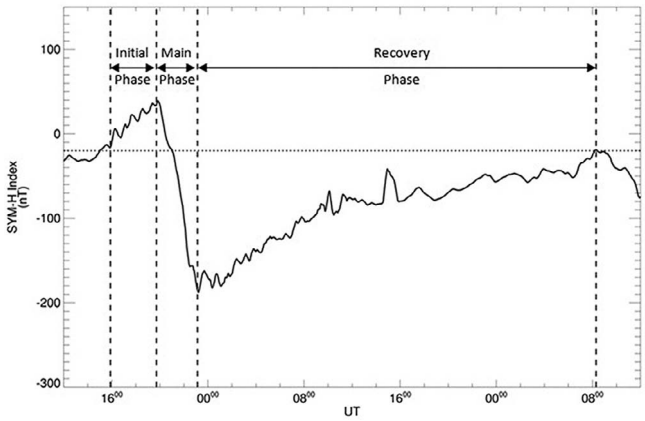

Figure 1. A characteristic *SYM-H* index storm trace showing initial, main, and recovery phases.

[7] Exact recovery processes are still unknown, though it is thought the bounce gyration frequency of ring current particles can couple to similar frequency ULF waves, and this can boost their energy and accelerate them out of the system causing scattering or precipitation. Generally speaking, tail reconnection and substorm activity can return the system to a more normal configuration over the period of a few days depending on the size of the storm [see review by *Gonzalez et al.*, 1994; *Daglis et al.*, 1999; *Liemohn et al.*, 1999; *Reeves et al.*, 2003].

[8] In this study we investigate the general features of storms by undertaking a superposed epoch analysis of geomagnetic storms over the last solar cycle (1997–2008) in order to investigate the correlation between solar wind driving conditions and the subsequent ring current enhancement seen in *SYM-H* evolution. We focus on the differences seen in CME- and CIR-driven storms, the controlling SW factors in the progression of storms and their storm phase durations. While a number of superposed epoch studies of storms have been completed in the past, we felt they did not take into account the largest storm size category (so-called superstorms) completely. We also chose to use a slightly different superposition technique, similar to one previous study undertaken by *Yokoyama and Kamide* [1997], that might give better alignment of like features for the superposition, see section 2.4. As such direct comparison of our results to those of *Yokoyama and Kamide* [1997] is presented. This work originates from a paper by *Milan et al.* [2009] that investigated the correlation between auroral oval radius and storm progression, also looking into the SW controlling factors of storms, and is intended to form a background to a future study using superposed ionospheric convection maps and auroral imagery to form a superposed statistical study that uses one of the widest data sources on storms to date.

2. Methodology

2.1. Identification of Storms

[9] In the last solar cycle (1997–2008), 143 geomagnetic storms were identified from their characteristic *SYM-H* variation as discussed in section 1. An automated, systematic approach was taken to identify all periods of *SYM-H* less than −80 nT and their subsequent recovery to "quiet" conditions of −15 nT; with the latter taken as the end of the recovery phase. The end of the main phase was identified as the minimum value of *SYM-H* reached. A minimum *SYM-H* value of −80 nT is somewhat larger than the minimum storm size of previous studies [e.g., *Taylor et al.*, 1994; *Yokoyama and Kamide*, 1997; *Zhang et al.*, 2006] but it was felt that would remove more erroneous detections of storms based on natural variations and any other phenomena that cause ring current intensity enhancements. Candidate events were then manually inspected to determine if they were correctly identified as storms; using both the knowledge of the characteristic storm *SYM-H* trace, and the requirement of corresponding enhanced SW and IMF conditions in the ACE OMNI data. The onset times of the initial and main phases were then selected manually. The initial phase was identified using the start of the solar wind enhancement, usually quite a sharp increase in activity, and the onset of the main phase by the sudden drop in *SYM-H* to negative values. This systematic approach ensured consistency, and any small errors induced by using a manual selection of the storm phase epochs were lessened by the process of averaging the storms. Attempts were made to use an automated routine, but due to the complexity and dynamic variation of individual events, the method above proved more robust at identifying all storms during this period. The 143 events that were identified were further categorized by size and onset solar wind conditions, discussed in sections 2.2 and 2.3.

2.2. Storm-Size Categories

[10] Storms were required to have a minimum *SYM-H* deflection of less than −80 nT, and then subsequently categorized as weak, moderate, and intense (see Table 1). These categories include more intense storms than previous studies have used [e.g., *Yokoyama and Kamide*, 1997; *Zhang et al.*, 2006], but it was felt that this would remove any chance of misidentification of weak storms compared to some other process that would cause a small increase in the ring current (e.g., reconnection events not associated with storms, substorms and oscillations in the location of the magnetopause), and better represent the most intense storms.

2.3. Identification of Onset Mechanism

[11] After locating storms over the last solar cycle, onset mechanisms were determined as broadly associated with either coronal mass ejections (CMEs) or co-rotating interaction regions (CIRs) using the ACE OMNI data compared to the "typical" signatures seen in Figures 2a and 2b [e.g.,

Table 1. Storm Size Definitions of This Study (in *SYM-H*) and a Previous Study by *Yokoyama and Kamide* [1997] That Uses *Dst*[a]

	This Study		*Yokoyama and Kamide* [1997]	
Category	Upper *SYM-H* Limit (nT)	Lower *SYM-H* Limit (nT)	Upper *Dst* Limit (nT)	Lower *Dst* Limit (nT)
Weak	−80	−150	−30	−50
Moderate	−150	−300	−50	−100
Intense	−300	–	−100	–

[a]*Dst* is approximately equal to *SYM-H* in magnitude at these values [*Wanliss and Showalter*, 2006].

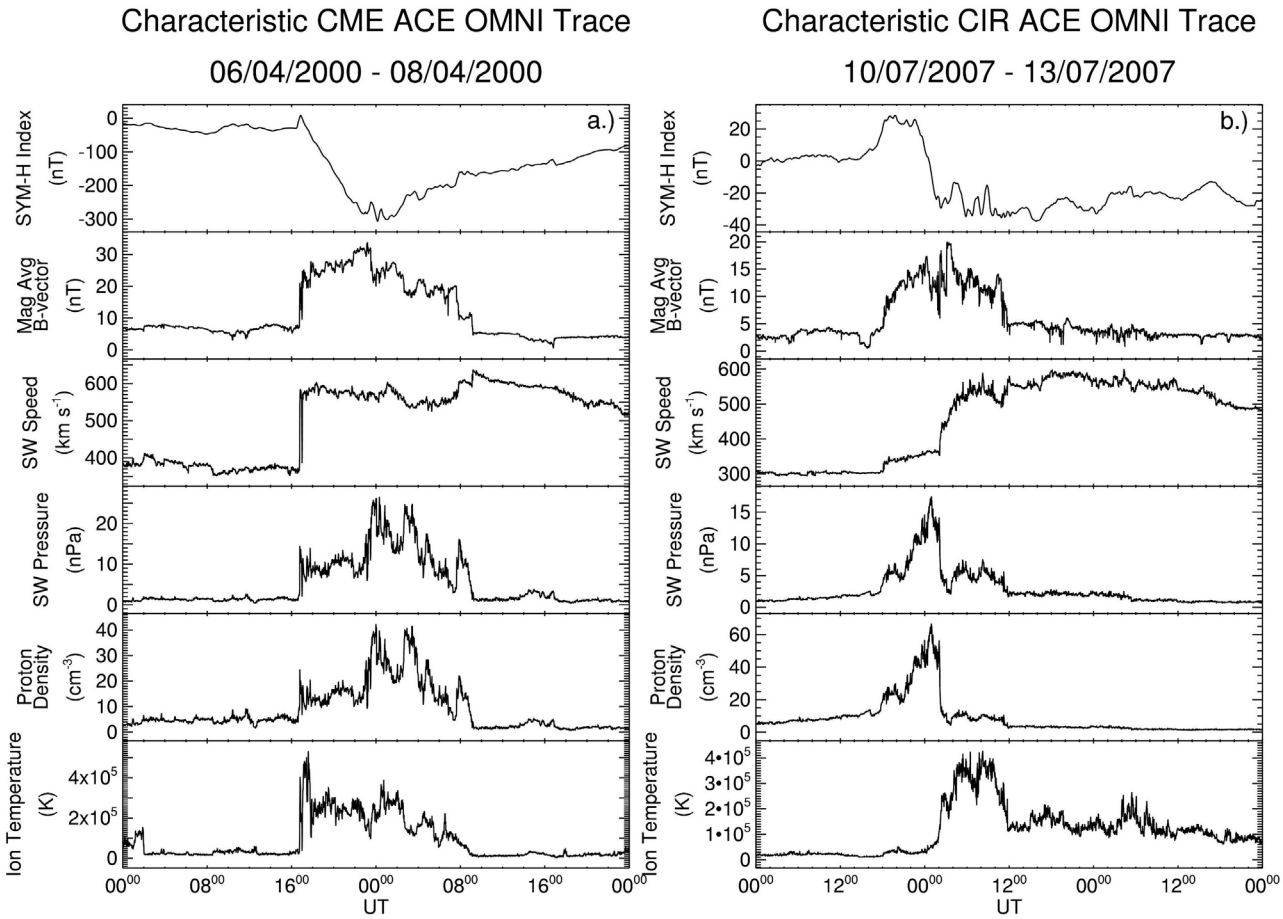

Figure 2. (a) A typical coronal mass ejection (CME) trace seen in ACE OMNI data, with simultaneous increases in all components: interplanetary magnetic field (IMF) magnitude, solar wind (SW) speed, pressure, density, and temperature. (b) A typical corotating interaction region (CIR) trace seen in ACE OMNI data, with simultaneous increases in IMF magnitude, pressure, and density, followed by subsequent decreases at the onset of increased SW speed and proton temperature.

Klein and Burlaga, 1982; *Neugebauer and Goldstein*, 1997; *Burlaga*, 1974; *Gosling and Pizzo*, 1999].

[12] A CME is an explosive ejection of plasma on a closed magnetic field loop from the solar corona. It is thought that magnetic reconnection occurs to pinch off the erupting bulge of plasma and field lines into a separate bubble, or CME, which then propagates out through the solar wind, either accelerating to the SW speed if slower, or causing a preceding shock if faster [*Gonzalez et al.*, 1999]. A CIR is caused by the combination of fast and slow flows in the SW. By Alfven's Theorem, the faster flow cannot pass through the slower flow and so a shock is formed in front of the compressed slow SW. These conditions associated with CIRs can then lead to a storm providing the there is a period of southward IMF B_Z [*Gonzalez et al.*, 1999].

[13] A CME signature is characterized as having simultaneous increases in SW speed, pressure, proton density and ion temperature, compared to a CIR signature that first has peaks in SW pressure and density, followed by subsequent rises in SW speed and temperature during decreasing pressure and density. Due to some gaps in the ACE data it was not possible to determine the onset mechanism for every storm in this study. While other onset mechanisms are known, including driver gas fields (e.g., magnetic clouds, flux ropes) and sheath fields (e.g., shocked heliospheric current sheets, draped magnetic fields) [*Gonzalez et al.*, 1994], the storms have been grouped by CME and CIR onsets in order to maximize their statistical significance.

2.4. Superposed Epoch Analysis

[14] During this study a superposed epoch analysis similar in method to *Yokoyama and Kamide* [1997] was employed. Rather than setting a common reference time (e.g., start of main phase) for each storm, t_0, to overlay and average the data, an alternative method using average durations was used, as described below and seen in Figure 3.

[15] Average duration of individual storm phases (initial, main and recovery) seen in Table 2, were found for the three size categories and then individual storm phases were adjusted to these normalized phase time indices, by shifting their data timestamps, to ensure common points in the storm progression were superposed. Common points on the storm *SYM-H* evolution were used to define the epochs of the individual phases as discussed in section 2.1, using the sudden increase in SW due to CME or CIR as the onset of the initial phase, the sudden turning of the *SYM-H* evolution

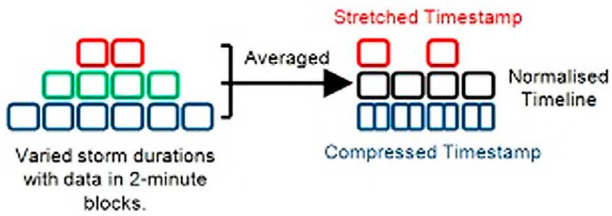

Figure 3. Diagram of the superposition technique used, finding average durations of individual storm phases and adjusting data timestamps prior to superposition.

to the rapid drop to negative values as the start of the main phase and the minimum negative deflection in *SYM-H* as the start of recovery which concluded when the *SYM-H* index returned to −15 nT.

[16] The start of each phase is essentially a common reference time for the superposition, but the adjustment of individual storm phase lengths to the average of the subcategory of the parent population is vital in ensuring good alignment in the superposition. This process was repeated separately on CME and CIR storms.

[17] This process allows a much more accurate picture of what an average, superposed storm looks like and is better at preserving any smaller features of individual storms from the main trend seen that could have been washed out in averaging processes if the storms are simply overlain. The superposition used the same 1-min time resolution bins in the normalized time period as was originally available in the *SYM-H* data. The process was repeated for all other auroral indices and SW parameters resulting in a complete superposed epoch analysis of storms by size and onset mechanism over the last solar cycle.

3. Observations

3.1. Distribution of Storms in the Solar Cycle

[18] The relationship between storm size and frequency was investigated, along with the monthly and yearly distribution of storms over the solar cycle. This was broken down further to incorporate the statistics of the onset mechanism of the storms, and is presented in Figures 4 and 5 and in Table 2. Figure 4a shows that the occurrence of storms decreases rapidly with increasing storm size, grouped into 20 nT bins. A biannual variation is seen in the monthly variation of storm occurrence, seen in Figure 4b, particularly in the more intense storms (moderate and intense) shown in red. And finally the frequency of storms with year (Figure 4c) shows a good correlation to that of the solar cycle activity with year in the form of sunspot number.

[19] Both of these results match previous studies, highlighted in the review paper by *Gonzalez et al.* [1994] and references therein, and gives us reassurance that despite the extended solar minimum and reduced activity of the sun over the past couple of years [*Livingston and Penn*, 2009], the last solar cycle storm variation is broadly similar to previous cycles. This similarity, combined with the results of *Wanliss and Showalter* [2006], which showed that over a large statistical survey the new *SYM-H* index could be taken as a de-facto high-resolution *Dst* index, allows direct comparison of the statistical results of this survey to those of much larger previous statistical surveys spanning many of the last solar cycles [e.g., *Taylor et al.*, 1994; *Yokoyama and Kamide*, 1997; *Zhang et al.*, 2006].

[20] Table 2 shows the direct comparison between storm size and storm driving mechanism of either CME or CIR. Only those storms which could be identified as either CME- or CIR-driven using the available OMNI data set were included. It is clear that intense storms and the majority of moderate storms are CME-driven, with only weak storms showing a significant proportion of CIR-driven storms. It is likely that this is due to the level of the SW-M coupling generated from a CIR storm compared to a CME storm. In particular, the variation of IMF B_Z with periods of increased SW ram pressure during a CIR storm results in reduced dayside reconnection and less intense driving of storms. This limits the size of the events compared to the more stable configuration of CMEs, which have a prolonged period of negative IMF B_Z to drive fast dayside reconnection and more intense storms. This is discussed further in section 3 and 4 where the relationship between storm duration, SW coupling and storm size are discussed in detail.

[21] Figure 5 shows the variation of CME/CIR storms throughout the year, normalized for storm occurrence. It is clear that CME-driven storms, being the dominant driver of storms in this study, closely follows the characteristic solar cycle activity variation, seen in sunspot number in Figure 4c. CIR storms occur at roughly a uniform rate throughout the solar cycle, though this is likely due to the selection criteria imposed on storm size removing small CIR-driven storms as CIR occurrence is known to peak during the declining phase of the solar cycle through to solar minima [*Tsurutani et al.*, 1995; *Denton et al.*, 2006].

3.2. Superposed Epoch Analysis Results

[22] A superposed epoch analysis was undertaken as discussed in section 2.4, with the results presented in Figure 6, where panels a, b and c show weak, moderate and intense storms respectively with no onset mechanism dependence (i.e., using the number of events from the "All" category in Table 2.). All plots are on a common time scale to allow direct comparison between events, but the *y* axis storm size scale is adjusted to show up all small scale features in the storm traces. As such it can be seen that weak storms have on average 4 times less intense ring current enhancement than intense storms.

Table 2. Results from the Superposed Epoch Analysis Showing the Average Size and Phase Durations for the Number of Storms in Each Size and Driving Mechanism Category

Category	Number of Events	Minimum *SYM-H* (nT)	Initial Phase Duration (min)	Main Phase Duration (min)	Recovery Phase Duration (min)
Weak	107	−105.7	487.5	523.5	2301.
Weak CME	73	−112.4	714.5	767.4	3372.
Weak CIR	34	−115.1	1534.	1647.	7240.
Moderate	28	−201.2	341.7	524.6	3177.
Moderate CME	25	−199.3	372.4	553.3	3268.
Moderate CIR	2	−171.3	115.5	350.5	3497.
Intense	8	−401.5	429.0	341.4	4862.
Intense CME	6	−372.8	468.8	365.7	5896.

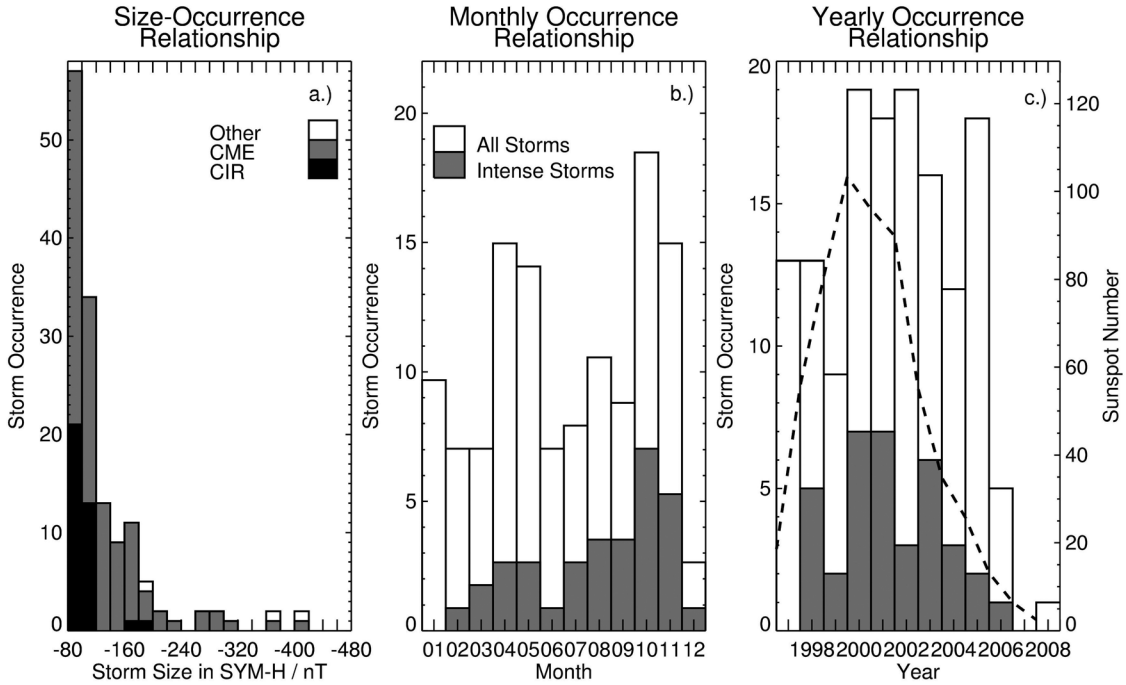

Figure 4. Geomagnetic storm occurrence: (a) storm size in relation to frequency of occurrence; (b) monthly variation in number of storms, with intense storms shown in gray; and (c) yearly variation in storm occurrence over the solar cycle, with the yearly sunspot number indicated by the dashed line.

[23] The common timescale is a measure of minutes from the onset of the averaged initial phases, with the duration of the storms equal to the sum of the periods of the averaged initial, main and recovery phases of that storm size category. As each phase is dealt with individually in the superposition method, and normalized in length such that the start and stop of each individual storm phase duration in that size category is adjusted and fixed to the ends of this normalized timeline, summing these timelines gives a common, normalized time index that allows direct comparison of the different storm size categories.

[24] Care must be taken in interpreting the superposed results due to the relatively small sample size of storms in general (see Table 2). This is particularly true for the most

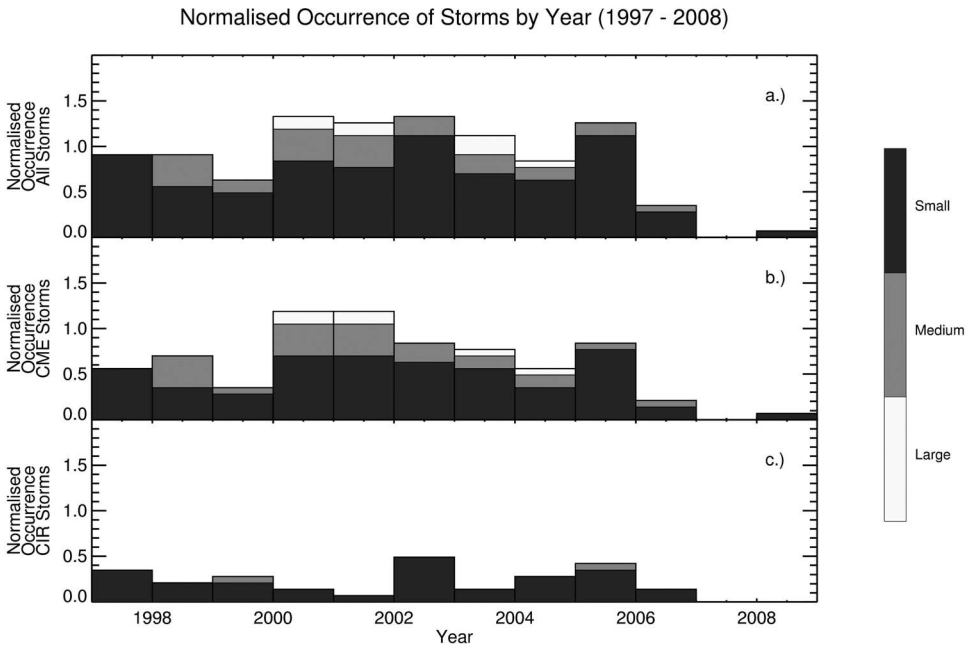

Figure 5. Normalized occurrence of storms per year to total number of events for (a) all storms, (b) CME storms, and (c) CIR storms.

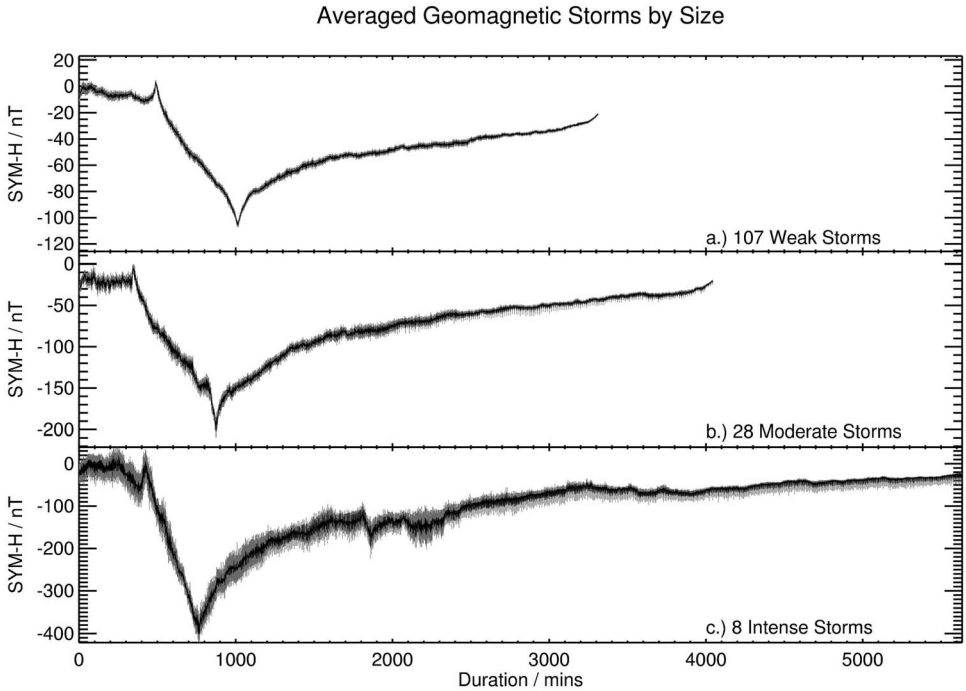

Figure 6. Superposed *SYM-H* storm traces for (a) weak storms, (b) moderate storms, (c) intense storms, on a common time axis but varying *SYM-H* scales.

intense events (8 in total) as less smoothing will have occurred due to the smaller number of events being averaged, compared to weak storms where more small individual variations in storms will have been smoothed out by the superposition technique. Any repeated feature at similar times during storms should still be seen though due to the alignment process in the superposition, (see section 2.4).

[25] Larger storms are also seen to have multiple minima in *SYM-H* during the progression of the main phase; usually due to a second major particle injection occurring leading to a further development of the ring current and second drop in *SYM-H* prior to recovery. Thus intense magnetic storms can often result from the superposition of effects of two closely separated moderate storms, and this is often seen in the corresponding SW data as having double structured southward IMF and dual peaks in SW pressure, density and speed [e.g., *Kamide et al.*, 1998; *Zhang et al.*, 2006; *Richardson and Zhang*, 2008].

[26] More intense storms are also often associated with multiple commencements, in the form of smaller storms or periods of strong dayside reconnection that can either hinder recovery, or give a small characteristic storm trace in the *SYM-H* index prior to the onset of the main event. In the case of prior storms, rapid recovery is often seen at the start of the initial phase of the intense storm, likely due to strong compression of the magnetosphere and magnetotail from the driving CME. However, these pre-storms can cause the start of the main phase to occur while there is negative *SYM-H* from the recovery of the previous event and some superposition of storms occurs as previously discussed. Hindered recovery prolongs the recovery phase duration and makes defining this period difficult for statistical analysis. In this case, overlapping storms were treated as one event, whereas storms occurring close to one another were called separate events assuming a complete initial, main and recovery phase was observed. This is seen in general from the separated storms and not purely from the superposed *SYM-H* trace. The famous "Halloween Storm" of 2003 [see *Gopalswamy et al.*, 2005, and references therein] is an example of this activity. This event was the largest storms seen in modern times and was in fact a double CME event, causing two storms close to one another, and a small storm prior to the first.

[27] There is evidence in all three storm sizes that there could be multiple recovery rates (first seen by *Akasofu et al.* [1963]), perhaps due to different species of ring current particle decaying at different rates, as suggested by *Hamilton et al.* [1988].

[28] Finally, Figure 6 shows the variation of storm phase duration with storm size, with identification of phases discussed in detail in section 2. It is reasonable to expect that smaller storms recover more quickly than larger storms as less energy has been transferred to the magnetosphere. It would also seem likely that small storms might have less intense initial phases (positive deviations in *SYM-H*) and shorter main phase durations than more intense events due to the length of energy input into the system limiting the size of the events, though this is not clear from Figure 6 and investigated further in section 3.3.

[29] Due to the limited sample size of CIR storms it is only possible to compare weak CME to CIR onset storms. This is seen in Figure 7, where there are clear differences between the two onset mechanisms. It should be noted that the CME storms have an artificially smoother *SYM-H* trace due to the number of events being averaged (~2 × CIR) and the fact there is less variation in the duration of the events making the superposition better. It is clear that the duration of both the main phase and subsequent recovery phase of

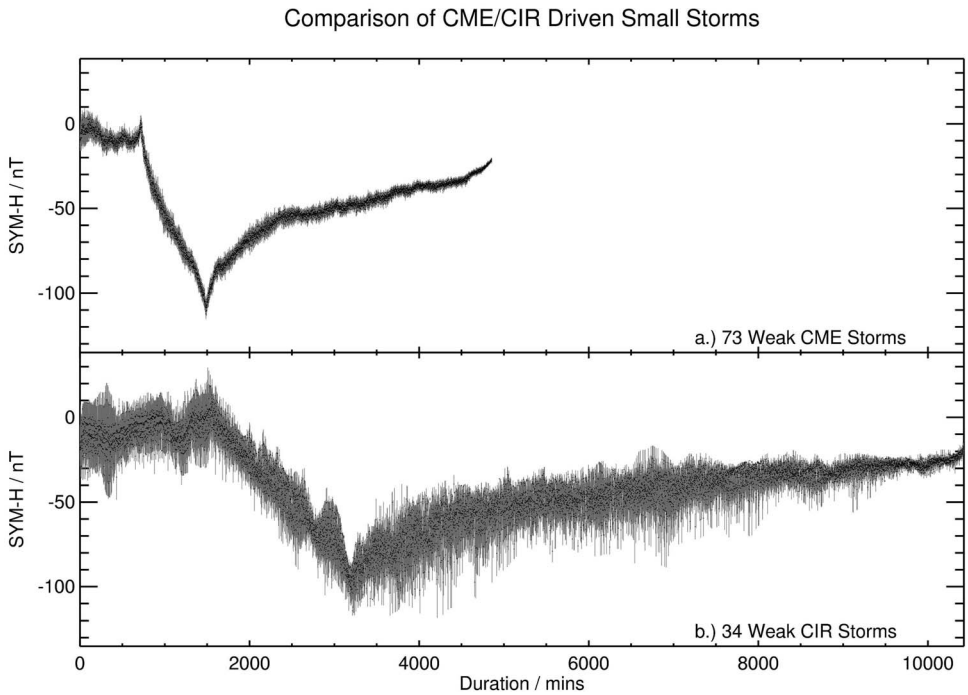

Figure 7. Superposed *SYM-H* traces for (a) CME-driven small storms, (b) CIR-driven small storms.

CIR-driven storms are much longer than those associated with storms driven by CMEs, with the CIR main phase trace having a much more gradual gradient to a more negative *SYM-H* value than that of the sharp decrease in CME main phase storms. Previous studies have described this as storm gradual commencement (SGC) and storm sudden commencement (SSC) [*Taylor et al.*, 1994], and it seems this can be attributed to CIR and CME onset mechanisms, respectively. Within the size category, the storm minima in *SYM-H* are roughly equal, suggesting the storm sizes are approximately evenly distributed for both CME and CIR events; however, CIR events are not seen for minimum *SYM-H* less than ~−150 nT, and this is a limiting factor in their "geoeffectiveness" compared to CME-driven storms, which can result in much more intense events.

3.2.1. Superposed Storm Solar Wind Conditions

[30] A superposed epoch analysis was also undertaken for the corresponding ACE OMNI data to accompany the corresponding *SYM-H* analysis for weak, moderate and intense storms. The superposed weak, moderate and intense storm results can be seen in Figures 8, 9, and 10, respectively. Standard errors of the samples are shown as gray regions around the averaged data points.

[31] It can be seen that small storms are generally associated with small enhancements in the solar wind pressure, density, speed and temperature with prolonged but small magnitude values (minimum −9.7 nT) of southward orientated (or negative values of) IMF B_Z. Little variation is seen in the other components of IMF, with B_Y of particular interest as it can induce slightly different reconnection morphologies [see *Cowley and Lockwood*, 1992]. It is reasonable to assume that any variations in these components on a storm-by-storm basis average out leaving a zero mean value, but we must still consider their magnitudes, particularly of IMF B_Y, as this is important in SW-magnetosphere coupling and could affect the development and size of geomagnetic storms. In general it can be seen that weak storms have smaller magnitudes of variations in the three IMF components.

[32] The combination of CME and CIR onsets makes it difficult to see the onset mechanism in the SW data panels. Limited auroral activity and substorm activity is seen in the auroral electrojet indices. A negative IMF B_Z is maintained throughout the period of the main phase, and it is this prolonged southward IMF that likely leads to prolonged dayside reconnection and drove the storm. The relatively small SW enhancements result in a correspondingly small storm, and it is clear that the IMF B_Z controls the progression of the main phase of the storm.

[33] Larger enhancements in the SW and IMF components are seen to create moderate storms compared to those for weak ones. The duration of negative IMF B_Z driving the storm is similar to that of weak storms, but at a more negative minimum value of −17.6 nT. It is likely that this combined with larger enhancements in SW pressure, speed and density result in more dayside magnetopause compression and correspondingly more rapid dayside reconnection driving in turn a larger storm. More variation in the IMF B_X and B_Y components is observed. This could be due to fewer storms resulting in imperfect averaging to a mean of zero. However, we see on a storm-by-storm basis an increase in the magnitude of these components for moderate and intense storms, suggesting more SW-magnetosphere coupling takes place. Enhanced substorm activity is seen in the auroral indices. Again the IMF B_Z is seen to be the controlling factor in the storm progression and was negative throughout the duration of the main phase.

[34] Intense storms are clearly driven by significantly more enhanced SW and IMF conditions than weak and moderate storms. The characteristic CME signature, simul-

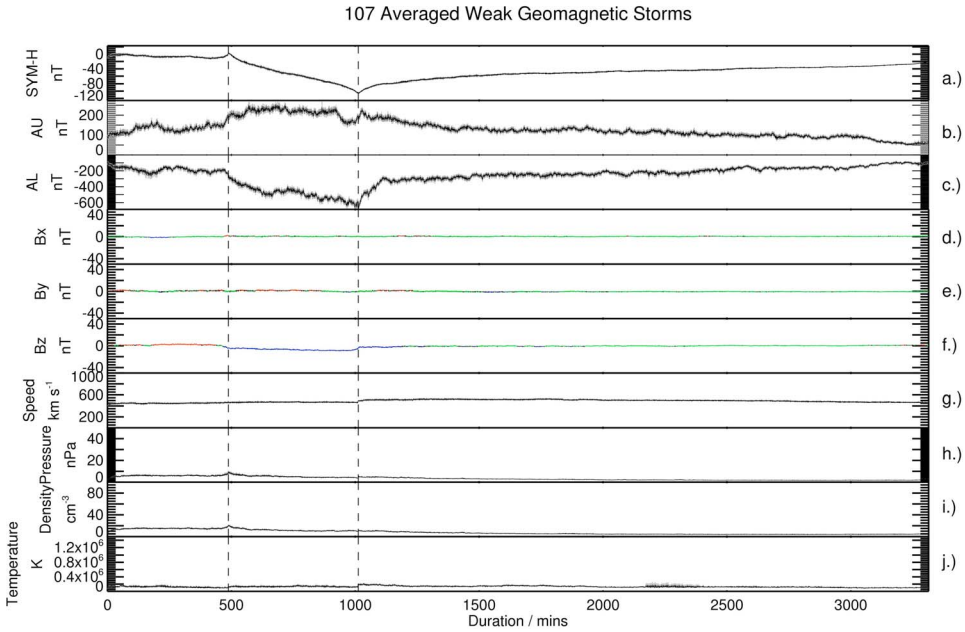

Figure 8. Superposed results for weak storms, showing *SYM-H*, *AU* and *AL* indices, IMF components, SW speed, pressure, proton density, and temperature.

taneous increases in SW speed, pressure, proton density and temperature with total IMF magnitude, shown in Figure 2a, can clearly be seen as the driving mechanism of the storm. The period of negative IMF B_Z is again seen to drive the storm and determine the duration of the main phase, however it is perhaps the magnitude of the IMF B_Z component, with a minimum value of −40.4 nT, that has the most dominant effect on storm size here as the period of southward IMF is seen to be less than weak and moderate storms. Much larger magnitudes of fluctuation in IMF B_Y is also seen by *Zhang et al.* [2006], and this increase will have added to the total magnitude of magnetic field enhancement, and likely intensified the coupling and driving of the system on the day side (see section 3.4). Auroral electroject indices are also greatly enhanced, suggesting stronger substorm activity. Recovery of the system takes much longer, but the duration of the main phase is also seen to be reduced compared to the other two storm size categories.

[35] This is investigated further in section 3.3 and 3.4, where SW-M coupling functions are used to estimate the

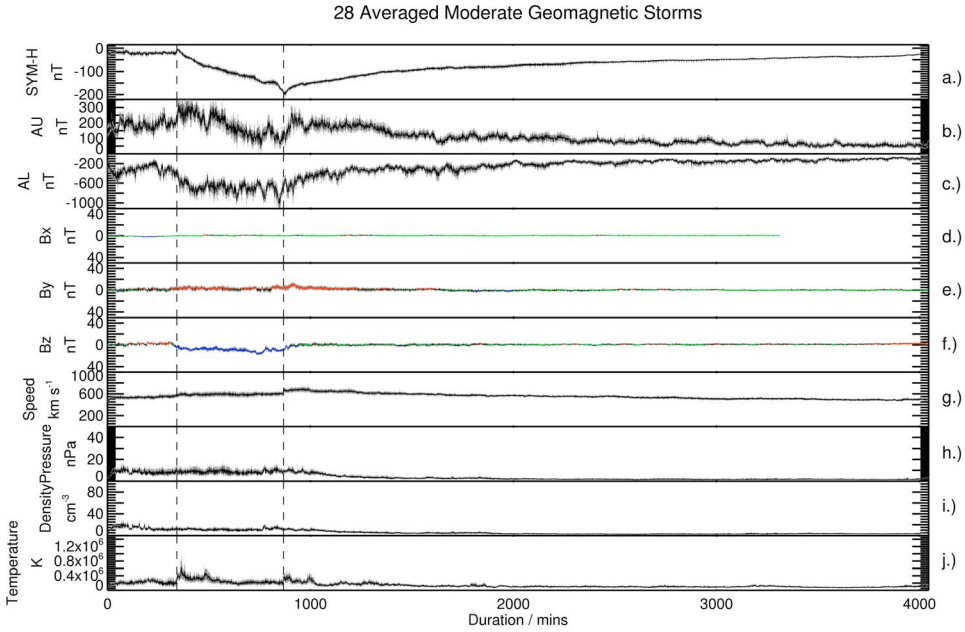

Figure 9. Superposed results for moderate storms, showing *SYM-H*, *AU* and *AL* indices, IMF components, SW speed, pressure, proton density, and temperature.

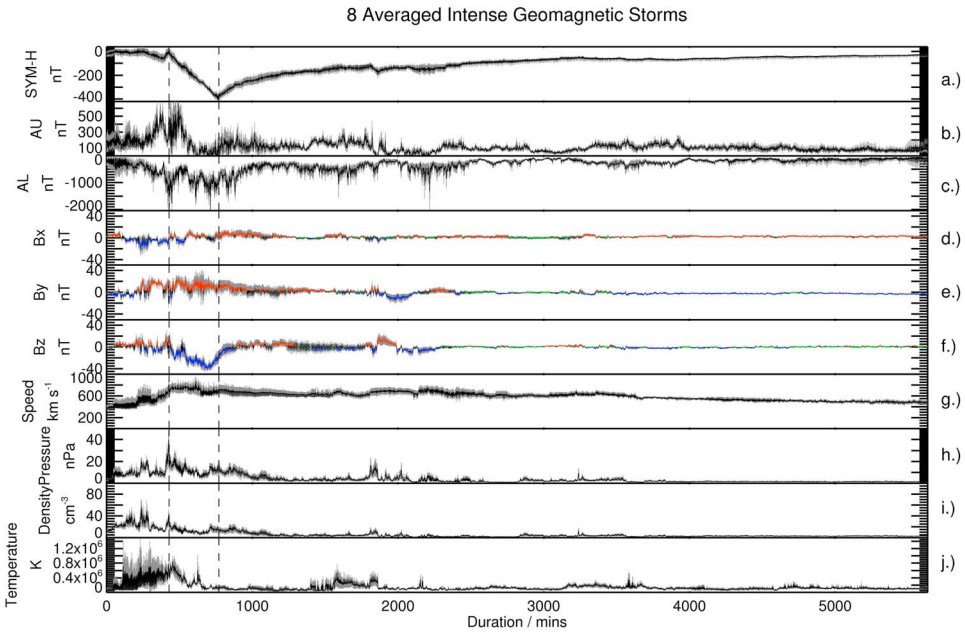

Figure 10. Superposed results for intense storms, showing *SYM-H*, *AU* and *AL* indices, IMF components, SW speed, pressure, proton density, and temperature.

energy input for each storm size group and their "geoeffectiveness". Further studies would be required to estimate the recovery rate during the driving of the main phase of storms and the subsequent rate during the recovery phase. These could be compared to standard SW-M coupling functions to gain a better understanding of the relationship between storm size in terms of ring current enhancement and storm phase duration with specific SW enhancement magnitudes and durations.

[36] The maximum/minimum respective variations in geomagnetic indices and SW enhancements for the three superposed storm size categories can be seen in Table 3.

3.3. Variation of Storm Phase Duration

[37] The variation of storm phase duration with storm size has been investigated before in a previous superposed epoch study by *Yokoyama and Kamide* [1997]. In contrast to the previous study, a new and unexpected relationship between the intensity of the storm main phase in the form of ring current enhancement and its duration has emerged and is reported here. The average phase durations for each storm size category can be seen in Table 2.

3.3.1. Initial Phase

[38] No clear relationship seen in the duration of the initial phase of the storm with storm size. This is likely due to the huge dynamic variations in CME and CIR structure and sizes. These result in variable durations of storm initial phases, the period of dayside magnetosphere compression before the IMF B_Z turns negative; the main controlling factor in the progression and onset of the main phase of a storm [*Kokubun*, 1972; *Taylor et al.*, 1994; *Yokoyama and Kamide*, 1997]. It should also be noted that the selection of the epoch of the onset of the initial phase is most subjective and liable to the largest error, due to the difficulties in choosing the point of sudden increase in SW properties associated with the CME or CIR prior to the main storm, and how to deal with situations where multiple commencements occur prior to the main event.

3.3.2. Main Phase

[39] Figure 11 shows the relationships between main phase duration and storm size for both this study and the study by *Yokoyama and Kamide* [1997]. *Yokoyama and Kamide* [1997] used *Dst* as the storm index showing ring current enhancement; however, *Wanliss and Showalter* [2006] demonstrated that *Dst* and *SYM-H* could be directly compared, with no more than 10–20 nT difference between the two for increasing storm intensity up to a maximum of −300 nT in *SYM-H*, where the simple combination of linear trends broke down. Thus a direct comparison of the results from *Yokoyama and Kamide* [1997] is possible, as Figure 11 shows. *Yokoyama and Kamide* [1997] used linear regression to fit a trend line through the first three storm sizes, calling the most intense storm duration an anomaly as it did not fit to the trend showing a clear tendency for the main phase duration to increase with storm magnitude. They also pointed out that when considering the

Table 3. Superposed SW Enhancements

Storm Size	Minimum *SYM-H* (nT)	Minimum B_Z (nT)	Maximum SW Speed (km s^{-1})	Maximum Pressure (nPa)	Maximum Density (cm^{-3})	Maximum Temperature (K)
Weak	−106	−9.7	537	9.6	20.4	2.1×10^5
Moderate	−201	−17.6	710	13.7	25.1	6.6×10^5
Intense	−402	−40.4	860	43.4	55.2	1.5×10^6

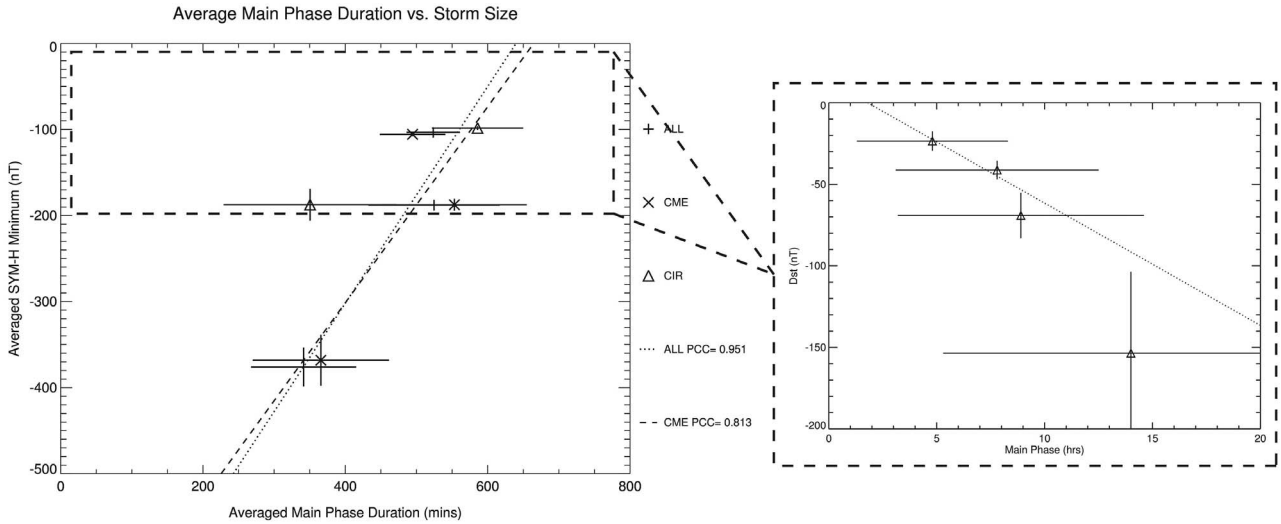

Figure 11. (left) Average main phase duration with storm size and onset mechanism, with (right) highlighted region showing previous results by *Yokoyama and Kamide* [1997]. Fitted lines used linear least squares regression, and Pearson's Correlation Coefficients are stated. Number of averaged storms in each size and driving mechanism category are given in Table 2.

data point associated with the most intense storms, that the intensity of magnetic storms tends to increase in a more than linear manner with main phase duration suggesting a more complicated, perhaps curved relationship than the linear trend presented [*Yokoyama and Kamide*, 1997]. Errors shown are the standard deviations for each category.

[40] A similar approach was used with the sample standard error for each category rather than standard deviation being employed as error bars. It is clear that, when taking into consideration more intense storms in separate storm size categories (moderate ($-300 < SYM\text{-}H \leq -150$) nT and intense ($SYM\text{-}H \leq -300$) nT rather than grouping all storms with $Dst \leq -100$ nT), the trend appears to reverse (Figure 11, left) and that main phase duration decreases with increasing storm size. By grouping all of the events with a ring current enhancement greater than −100 nT in *Dst*, *Yokoyama and Kamide* [1997] would not have been able to see this and treated the data point as anomalous compared to the linear trend they saw for their smaller storm classifications. Linear least squares was used to fit the lines of best fit for CME and ALL storms combined, with the Pearson's Correlation Coefficient (PCC) showing very good fits. Due to the limited number of more intense CIR storms, it is not possible to fit a line of best fit.

[41] In order to better determine the relationship between storm size and main phase duration and develop this new trend further, the data were re-binned into smaller size categories, seen in Figure 12. By using smaller storm size categories the trend is better shown, but each category then have a smaller number of storms averaged in it, increasing the statistical uncertainty and giving larger error bars on Figure 12. The number of storms in each category can be seen in Table 4.

[42] The small storms in this study appear to follow the results of the previous work by *Yokoyama and Kamide* [1997], however there is a departure from this trend beyond storms around ∼−150 nT, whereby main phase duration decreases with storm intensity. The main phase duration is seen to be closely correlated with the duration of southward IMF B_Z, such that the question is not how storm size and main phase duration affect one another but rather why does a specific storm size in *SYM-H* occur for a given main phase duration; with the magnitude of SW enhancement driving the storm, and therefore the amount of SW-M coupling, likely to be important. It would make sense for a longer main phase duration (and therefore period of southward IMF B_Z) to be required for bigger storms, i.e., it would take longer to reach a more negative value of *SYM-H* as seen by *Yokoyama and Kamide* [1997], but Figure 12 shows this not to be the case. In order to try to replicate the trends seen in Figure 12, as an over simplification we can think about the relative rates of ring current excitation (R_{RCE}) and ring current recovery (R_{RCR}) that would be required. Obviously the exact physical processes that are occurring are more complicated and not yet fully understood, as are the relationships between R_{RCE} and R_{RCR}, but in this paper we attempt to suggest possible reasons for the trends of Figure 12, and propose these as the subject of future study.

[43] Figure 15 shows that enhanced SW-M coupling occurs for increasing storm size in minimum *SYM-H*. It is perhaps reasonable to assume that the ring current becomes more enhanced, and at a quicker rate (R_{RCE}), for increased SW coupling, and that associated with this enhanced ring current, the recovery rate (R_{RCR}) is also increased. If increases in R_{RCE} and R_{RCR} remain proportional for increasing storm size and therefore SW enhancement, ring current energy and population density, then a linear trend of increasing storm size requiring longer duration enhancement becomes practical. However, this is not observed to be the case for all storm size categories, with suggestions as to why this trend reverses found in section 4 using the idea of an imbalance in R_{RCE} and R_{RCR} with increasing storm size and coupling.

[44] It should be noted that the main phase durations (and those of the recovery phase in section 3.3.3) are scaled lengths, due to the nature of the superposition to the average period of the storm phase in a given storm size category;

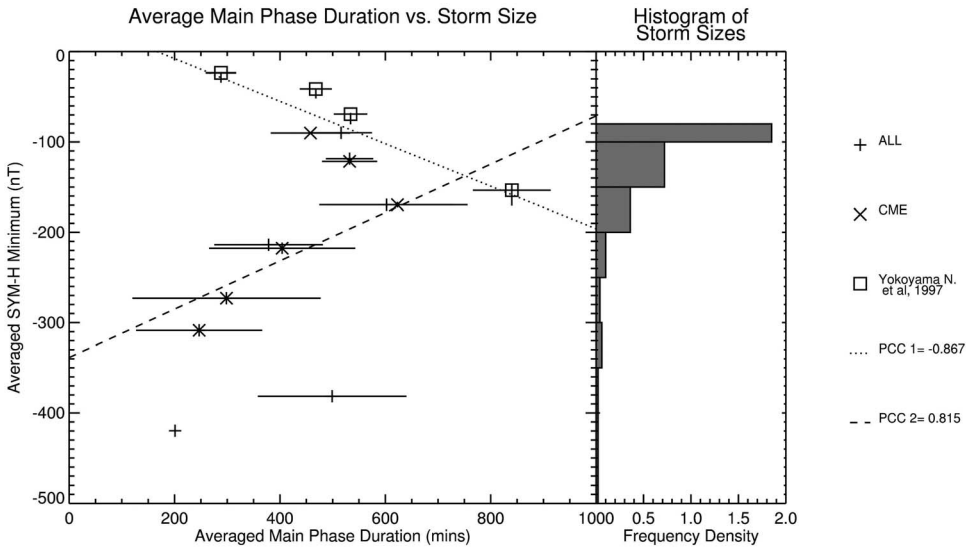

Figure 12. Average main phase duration with storm size and onset mechanism, re-binned into smaller size categories to show the overall trend compared to previous results by *Yokoyama and Kamide* [1997]. Fitted lines used linear least squares regression, and Pearson's Correlation Coefficients are stated. Number of averaged storms in each size and driving mechanism category are given in Table 4.

however this is directly comparable to the method used by *Yokoyama and Kamide* [1997] and shows the average duration of the main (or recovery) phase of storms within a given size range in minimum *SYM-H*.

[45] Lines of best fit using linear least squares regression are included to show the two trends seen. The upper trend uses all of the data from the study by *Yokoyama and Kamide* [1997] and CME storms for *SYM-H* > −200 nT. The second trend uses the data from *Yokoyama and Kamide* [1997] and CME storms for *SYM-H* < −100 nT. The two most intense storms were not included because they had missing OMNI data and could therefore not be classified as either CME or CIR. It is likely that there is a nonlinear relationship between storm size in minimum *SYM-H* and main phase duration and not the two linear trends shown here to emphasize the two regimes. Some of the points for more intense storms have a smaller statistical significance due to the number of events that are averaged and so should be treated carefully (see Table 4).

3.3.3. Recovery Phase

[46] The results of *Yokoyama and Kamide* [1997] are again overlaid onto the results of this study in Figure 13. It can be seen that there is a close match between the two, particularly for the CME-driven storms. It is likely that this is due to CME storms dominating the sample population used by *Yokoyama and Kamide* [1997] because they did not treat the driving mechanisms separately, resulting in the average durations for both main and recovery phases having a better correlation with our CME storms. Linear least squares regression is again used to fit the lines of best fit and the Pearson's Correlation Coefficients are shown which indicate a good fit. It is reasonable to assume that statistically similar distributions of storms occurred in this solar cycle compared to the last examined by *Yokoyama and Kamide* [1997]. This is seen in the similarity in storm occurrence variations with year and month to previous studies (section 3.1), and in the similarity of recovery phase durations in this study to those of *Yokoyama and Kamide* [1997]. This in turn adds weight to the argument that the new trend seen in the main phase duration with increasing storm intensity is valid and not a random variation in this solar cycle.

[47] This trend is again extended in Figure 14, where the same smaller storm size categories are used as in section 3.3.3. The line of best fit again shows the good correlation between the results of *Yokoyama and Kamide* [1997] and the CME-driven storms in our study.

3.4. Storm Size to Solar Wind Coupling

[48] Various SW-magnetosphere coupling functions have been previously suggested [for a review, see *Gonzalez et al.*, 1994], in order to try and link SW conditions with storm size and progression, with a number of them reproduced in Figure 15. The coupling functions were calculated for each 1 min resolution data-point during the main phase of each storm and then averaged together based on storm size using the same categories as before. While the simple coupling function, (panel a), of solar wind speed multiplied by IMF B_Z component gives the best PCC of 0.9996, more realistic

Table 4. Number of Storms in the Rebinned Storm Size Categories Used to Better Establish the New Trend Seen in Main Phase Duration With Increasing Storm Size

SYM-H (nT)	−80 to −150	−150 to −200	−200 to −250	−250 to −300	−300 to −350	−350 to −400	−400 to −450	−450 to −500
CME	37	18	5	2	3	1	1	1
All	57	19	7	2	3	2	2	1

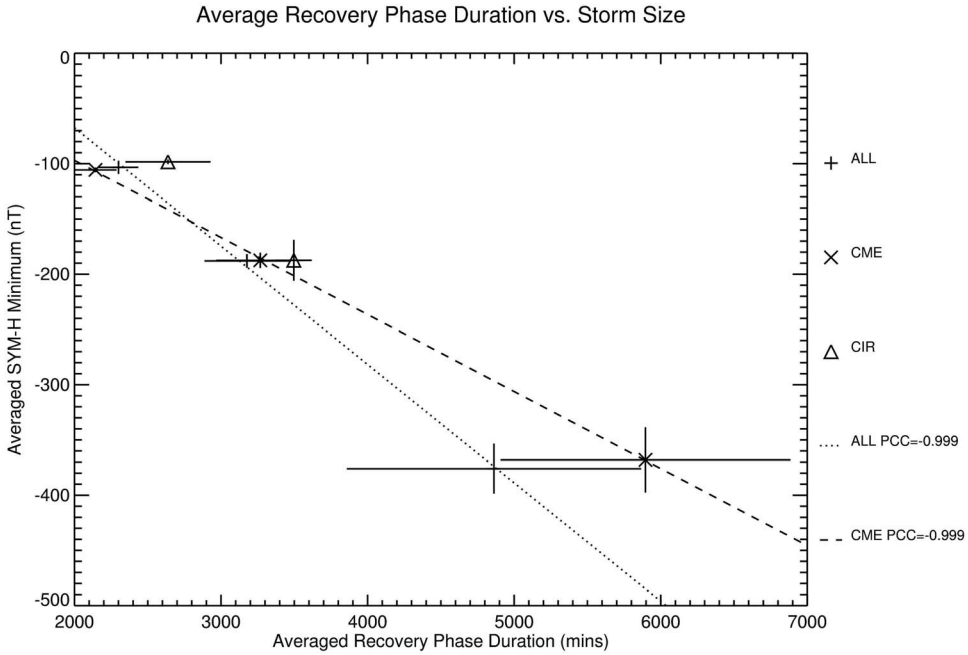

Figure 13. Average recovery duration with storm size and onset mechanism compared to previous results by *Yokoyama and Kamide* [1997]. Fitted lines used linear least squares regression, and Pearson's Correlation Coefficients are stated. Number of averaged storms in each size and driving mechanism category are given in Table 2.

functions involving more SW and IMF parameters as well as the solar wind clock angle, θ, also give good results. Of particular interest is panel g, which uses the function given by *Milan et al.* [2009], which was shown to give a good estimate of the dayside reconnection rate and also developed the understanding of the storm size, auroral oval radius and reconnection rate relationships, and can be seen here to give a good PCC value of −0.9591. It must be said that these results do not always hold true on an individual storm-by-storm basis, as there can be reasonably large variations in coupling function values calculated from storm time SW conditions for all coupling functions that were investigated. This means the very good correlations presented in Figure 15 are due to looking at the "average" SW conditions and storm

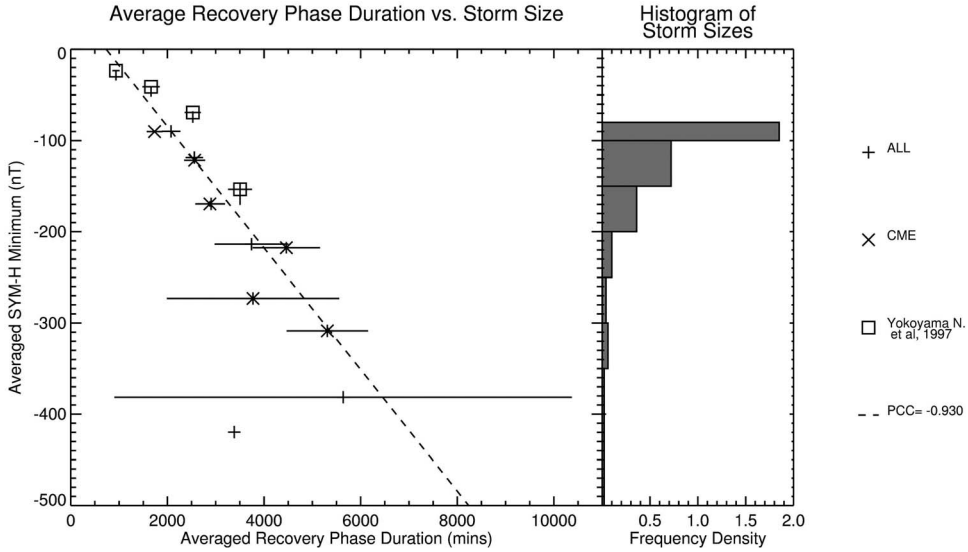

Figure 14. Average recovery phase duration with storm size compared to the previous results of *Yokoyama and Kamide* [1997], using the smaller storm size categories of section 3.3.3 and Figure 13 to better determine the trends seen. Fitted lines used linear least squares regression on the CME and *Yokoyama and Kamide* [1997] data points, and Pearson's Correlation Coefficients are stated. Number of averaged storms in each size and driving mechanism category are given in Table 4.

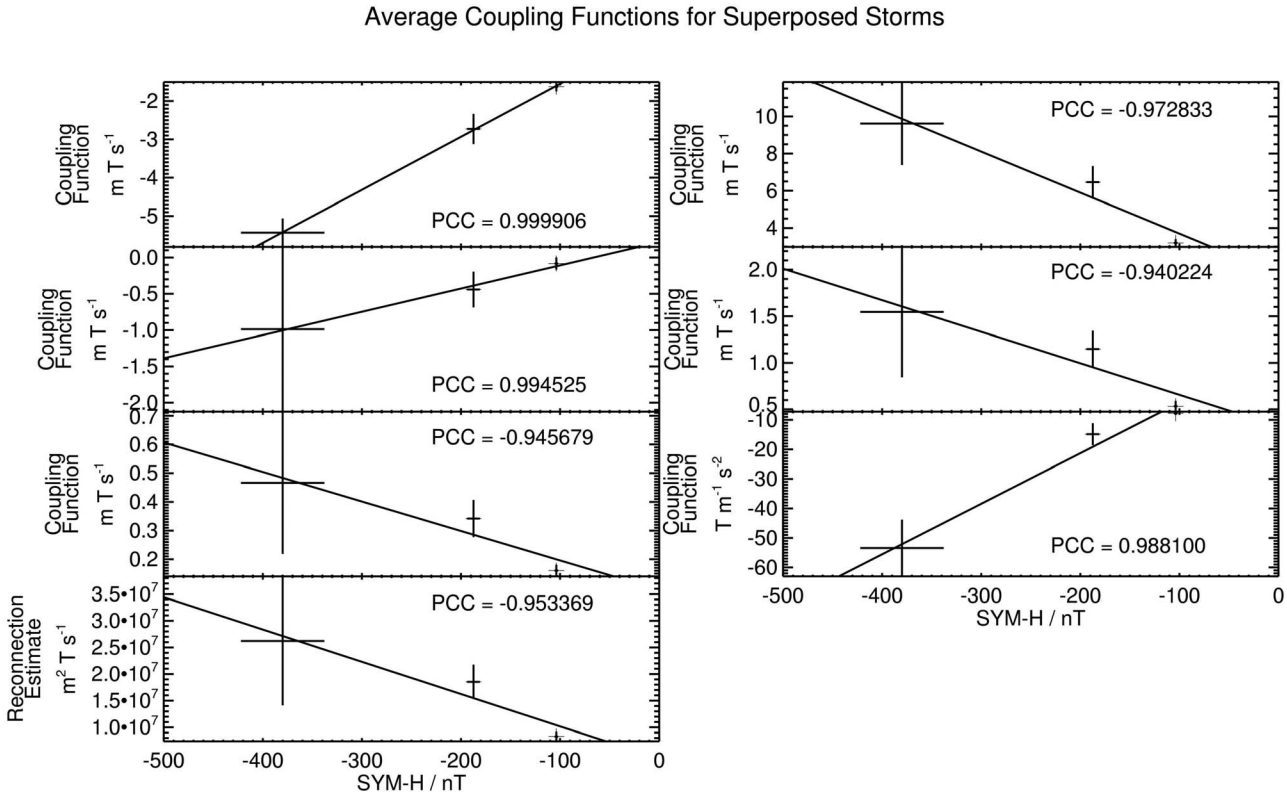

Figure 15. Average coupling functions for superposed storm size categories, all with linear least squares regression fitted lines of best fit and stated Pearson's Correlation Coefficients. Coupling functions (see *Gonzalez et al.* [1994] for review) are:(a) $v_{sw}B_z$, (b) $v_{sw}B_T$, (c) $v_{sw}B_T\sin\left(\theta/2\right)$, (d) $v_{sw}B_T\sin^2\left(\theta/2\right)$, (e) $v_{sw}B_T\sin^4\left(\theta/2\right)$, (f) $n_{sw}v_{sw}{}^2B_z$, (g) $2.75R_Ev_{SW}\sqrt{B_y^2+B_Z^2}\sin^2\left(\theta/2\right)$.

size in *SYM-H* minima after superposition. The same is true for the storm phase duration with storm size, where individual events can fall a long way from the main trend seen with averaged events. The superposed epoch analysis results can give us a good understanding of the general relationships and variations of geomagnetic storms, whereas individual events are naturally going to deviate from this trend due to the very variable nature of geomagnetic storms; one of the things that makes predicting storms and space weather so difficult and important. Those individual events that deviate from the average trends seen are more likely to be extreme, and could be studied individually (e.g., 2003 Halloween Storm, see *Gopalswamy et al.*, 2005 and references therein).

4. Discussion

[49] The results of a superposed epoch analysis of the geomagnetic storms over the last solar cycle (1997–2008) have been presented. Storms are a fundamental phenomenon in geophysics that despite being studied for over 50 years, are still not fully understood. This study gives new insights into the complicated coupling between the SW and storm size and development.

[50] 143 storms over a 12 year period have been analyzed using a systematic semi-automated approach. Storms were identified by their characteristic *SYM-H* index evolution and onset mechanism found from in situ upstream SW measurements from the ACE OMNI data set. Storms were classified as weak ($-150 < SYM\text{-}H \leq -80$) nT, moderate ($-300 < SYM\text{-}H \leq -150$) nT and intense ($SYM\text{-}H \leq -300$) nT.

[51] Of the 143 storms found, only 36 were CIR-driven, which were generally all weak storms. One hundred and four were found to be CME-driven, and these dominate all of the groups and were the only onset mechanisms found for the most intense storms. It is likely that more, smaller CIR-driven storms could be found by extending the storm size criteria above −80 nT as a minimum and that the occurrence of those would then follow the known trend of peaking during solar minimum years [*Tsurutani et al.*, 1995; *Denton et al.*, 2006], rather than reflecting the almost constant level seen throughout the solar cycle in this study. The monthly and yearly variation of storm occurrence (Figure 4) matched the results of previous long duration statistical studies of storms [e.g., *Taylor et al.*, 1994; *Yokoyama and Kamide*, 1997; *Zhang et al.*, 2006]; with a diurnal variation seen in the monthly variation of intense storms [see review by *Gonzalez et al.*, 1994, and references therein], and the yearly variation closely following that of the solar cycle activity in the sunspot number [e.g., *Gonzalez et al.*, 1994].

[52] Storms were superposed by size, onset mechanism, and individual phase, in a method similar to that of *Yokoyama and Kamide* [1997], using the average duration of each phase in each category to form a normalized timeline to

which storms were superposed. This allows common points in a storm progression to be overlaid despite them having different durations, and maintains more of the small scale details of storm progression than a simple method of overlaying storms based on a common reference point (e.g., start of the main phase). This method was repeated for each storm size and onset category.

[53] As might be expected, more intense storms are associated with more extreme enhancements of the solar wind. Weak storms were found to be on average 4 times smaller in terms of their *SYM-H* variation than the average intense storms. All storm main phases were associated with a prolonged negative period of IMF B_Z with increased SW ram pressure driving fast dayside reconnection, and end with the IMF B_Z component becoming less negative or positive. Storm progression was seen to be strongly IMF B_Z dependent assuming maintained enhanced SW conditions. More extreme storms also had correspondingly larger enhancements in the auroral electrojets and more substorm activity. Multiple enhancements of the ring current, along with corresponding drops in the *SYM-H*, during the main phase of moderate and intense storms were also common, as well as smaller events before and after the main large storm [e.g., *Kamide et al.*, 1998; *Zhang et al.*, 2006; *Richardson and Zhang*, 2008]. There is some observational evidence of two different recovery rates. *Hamilton et al.* [1988] suggested this might be due to two distinct ion species decaying at different rates, though further analysis of the recovery periods using in situ particle measurements would be needed to confirm this, perhaps from the Los Alamos National Laboratory geostationary spacecraft [e.g., *Jordanova et al.*, 2001] or future radiation belt missions, such as NASA's Radiation Belt Storm Probe (RBSP) mission due for launch in 2012 [*Liemohn and Chan*, 2007] and the European Space Agency's Orbitals mission due in 2013.

[54] The relationship between storm size and phase duration was investigated, with a particularly interesting result seen in the main phase duration compared to previous studies. The storm main phase duration was generally seen to decrease with increasing storm size compared to previous results showing the opposite trend.

[55] No relationship was found between the initial phase duration and storm size. It would seem the initial phase terminates and the main phase begins with the onset of prolonged negative IMF B_Z, and the variation in the magnetic structure of CMEs and CIRs is likely to be so large that the initial phase duration and storm size should be uncorrelated. Selection of the epoch of the onset of the initial phase is also most subjective and has the largest error due to the difficulties in selecting the sudden onset of enhanced SW properties associated with the CME or CIR driving the storm.

[56] The trend between main and recovery phase duration and storm size had been investigated previously by *Yokoyama and Kamide* [1997], who showed for both cases that phase duration increased linearly with storm size; though they deemed their most intense storm category as anomalous. Using different classifications of storm size, this study shows that these results match the previous study for main phase duration up to a critical point of ~−150 nT, after which the trend is seen to reverse and main phase duration decreases with increasing intensity of the largest storms. We have seen a very clear correlation from Figures 8, 9, and 10 that the main phase duration is driven by the time period that IMF B_Z remains negative in the SW. This leads to the interesting question of why, for a short period of "favorable" SW conditions, can either a very weak or most intense storm occur, seemingly with no variations in-between?

[57] The first stage of the trend observed in Figure 12, which is similar to that of *Yokoyama and Kamide* [1997], is as you might expect. It displays increasing main phase duration with more negative *SYM-H*; or in other words more intensification of the ring current requiring a longer duration of driving and SW coupling which is controlled by the duration of southward IMF B_Z. It is reasonable to suppose that for this increase to occur, a combination of a small magnitude but longer duration of SW enhancement would be required and this is seen in the superposed ACE OMNI data. Given the increase in SW-M coupling that occurs (Figure 15), it might be reasonable to assume that any increase in ring current excitation rate (R_{RCE}) due to the increased coupling is countered by a roughly though perhaps not precisely proportional increase in ring current recovery rate (R_{RCR}).

[58] Beyond the turning point in the relationship at ~−150 nT, it is possible that the magnitude of the SW enhancement, in particular the increasingly more extreme negative values of IMF B_Z seen for increasing storm size categories, becomes the most important in determining how much SW-M coupling can occur in the observed shorter main phase durations. This could be a controlling factor of the storm size in terms of possible ring current enhancement and minimum *SYM-H*, and also shows a tendency for extreme enhancements to be short-lived in the SW. It is proposed that these conditions could cause a disproportional increase in the R_{RCE} and R_{RCR}, allowing a more negative *SYM-H* value to be achieved in a shorter duration if R_{RCE} were to dominate the associated R_{RCR} (increase in R_{RCE} > increase in R_{RCR}). Whether or not the R_{RCR} is just saturated by the increase in excitation, or alternatively tends toward a maximum rate will be the subject of a future study, where we hope to develop this possible relationship further by comparing gradients in *SYM-H* during the recovery phase to SW conditions and *SYM-H* value. It is clear however that this is unlikely to be two distinct linear trends presented in Figure 12, but more likely a gradual, nonlinear transition and could be highlighting the imbalance of driving and recovery of the ring current enhancement from smaller *SYM-H* values than the reversal stated here at ~−150 nT. In any case, this result poses important implications on predicting the effects of space weather and the terrestrial geospace response to given SW conditions.

[59] A larger study, likely involving storms from multiple solar cycles, would be needed to increase the number of events in each storm size category and increase statistical significance, confirming this trend. Proposed future work includes finding a better estimation of the net ring current energy injection by finding decay rates to compare to the estimates of reconnection and injection rates given by SW-M coupling functions. This is likely to use in situ spacecraft data of plasma density and energy, and images of the auroral oval as a guide to ring current enhancement, using methods of *Milan et al.* [2009]. Ring current recovery rates (R_{RCR})

and decay constants can also be estimated using energy balance equations and durations of recovery phases, though this requires simplifications and is limited to assuming linear recovery rates [see review by *Gonzalez et al.*, 1994].

[60] The recovery phase duration with storm size is seen to closely follow the results of the previous study, which combined with the "typical" size, monthly and yearly variations in storm occurrence, suggests similar events were seen in this study as the previous solar cycle and direct comparison is permissible. It is suggested that main phase duration should increase with storm size until a point at which the corresponding recovery rate maximizes, beyond which SW enhancements are so intense that they drive the main phase to its minimum at quicker rates.

[61] Finally, correlations of SW enhancements to storm size using various previously suggested coupling functions have been reported [see review by *Gonzalez et al.*, 1994, for more details]. Understanding how ring current enhancement and enhancements in solar wind are correlated is required for both the safe maintenance of spacecraft and proposed human spaceflight throughout the next solar cycle. All coupling functions tested showed a good correlation to storm size, but only using the averaged superposed storms; actual storms showed large variation and gave poor Pearson's Correlation Coefficients to lines of best fits put through the data. Some coupling functions, such as the one suggested by *Milan et al.* [2009] have been shown to link storm size and auroral oval radius, and these more "physically realistic" coupling functions compared to simpler early ones involving linear combinations of SW properties should be developed further to better link all the geophysical phenomenon that occur during storm times.

[62] The next stage of this study will involve using radar data from the SuperDARN network in conjunction with auroral images from IMAGE and POLAR to produce corresponding superposed ionospheric convection patterns for the storms presented here. An investigation of these ionospheric convection patterns will give more information on processes leading to ring current enhancement and further our understanding of the complicated coupling that occurs between the solar wind, magnetosphere and ionosphere during these periods. The excitation and subsequent recovery of the ring current will also be investigated using in situ particle measurements and radar data to look for excitation wave modes.

5. Conclusion

[63] A superposed epoch analysis of 143 storms over the last solar cycle (1997–2008), (104 CME and 36 CIR), was completed; with the storms found from their characteristic *SYM-H* trace and corresponding driving mechanism in the SW found in ACE OMNI data. Storm occurrences were found to have a biannual distribution, and closely follow the solar cycle activity variation seen in sunspot number.

[64] Based on the storm size categories, weak ($-150 < SYM\text{-}H \leq -80$) nT, moderate ($-300 < SYM\text{-}H \leq -150$) nT and intense ($SYM\text{-}H \leq -300$) nT, it was found that intense storms experienced a ring current enhancement 4 times that of weak storms. Corresponding SW enhancements were also shown to be significantly stronger for intense storms, though they lasted for shorter periods than weaker events, suggesting a greater energy transfer into the system for short extreme enhancements than prolonged weak ones.

[65] Direct comparison between weak CME- and CIR-driven events showed larger main phase durations for CIR storms than CMEs. It is suggested that CIRs are more likely to be responsible for storm gradual commencement events (SGCs) and CMEs for storm sudden commencement events (SSCs), using the notation of *Taylor et al.* [1994]. Again this suggests that despite CIR SW enhancements lasting for longer periods than CMEs, their relatively smaller increase causes less SW-M coupling and transfers a smaller amount of energy into the system.

[66] The duration of individual storm phases was investigated with increasing storm size, showing a new and interesting trend in the main phase duration. No trend was seen in the length of the initial phase with storm size, as may be expected as it is shown that this is mainly controlled by the IMF B_Z orientation in the CME/CIR; and that a prolonged southward IMF B_Z initiates the main phase of the storm.

[67] A previous study by *Yokoyama and Kamide* [1997] showed that main phase duration linearly increased with storm size. Our results, using different storm size categories to better show the duration of larger events, shows on average the opposite is true. We see the main phase duration decrease with increasing storm size. This is further emphasized after re-binning the data into smaller storm size categories, being careful of the statistical significance, whereby a break between the two trends is seen for storms at ~−150 nT. Before this point, our events closely match (Pearson's Correlation Coefficient of −0.837) the trend described by *Yokoyama and Kamide* [1997], which shows increasing duration with storm size, after which the trend reverses (Pearson's Correlation Coefficient of 0.939). It is proposed that the relative magnitude to duration of SW enhancement is important in determining how large, in minimum *SYM-H* excursion, a storm can become. It is also possible that in order to get the two distinct trends observed in Figure 12, given that the duration of the main phase is strongly correlated to the period of negative IMF B_Z, that the ring current recovery rate (R_{RCR}) gets dominated by the excitation rate (R_{RCE}) beyond ~−150 nT. That is to say that the R_{RCR}, by relaxation or particle loss, could increase with increasing energy input to either tend toward a maximum or simply increase in such a way that it is saturated by the R_{RCE} for a given SW enhancement and amount of coupling. Thus the most intense events would only require a short duration of extreme SW enhancement, while still allowing weak and moderate events to be formed from reasonably small magnitude but prolonged SW enhancements; and hence create the dual trend observed. It should be noted that no examples of prolonged extreme conditions in the SW were observed, only on average shorter durations for increasing enhancement, perhaps identifying a limiting factor in the ratio of size to duration of CMEs and ultimately the maximum ring current enhancement, or *SYM-H* minimum possible. It should be noted that discussing ideas of relative rates of ring current enhancement and recovery is a dramatic simplification of the complicated and still not fully understood physical processes involved but can give plausible reasoning for both the *Yokoyama and Kamide* [1997] and reversal trends presented in Figure 12. Also, although the phase durations

are scaled lengths due to the method of superposition employed, that does not inhibit comparison with the results of *Yokoyama and Kamide* [1997] who used a similar procedure, and shows the average durations and SW enhancements for a given storm size category defined by *SYM-H* minimum. Due to their global nature and varying driving conditions in the SW, geomagnetic storms can vary quiet significantly on an individual storm basis, making space weather forecasting a difficult proposition. However, examining the average trend of storm size from the duration and size of the SW and IMF enhancements over the last solar cycle can prove useful.

[68] Recovery phase duration is shown to increase with storm size in agreement with the observations of *Yokoyama and Kamide* [1997], confirming that a more enhanced ring current takes longer to decay, though this trend may not be linear. The exact relationship between storm size, ring current excitation rate and associated recovery rate requires further investigation. Various SW-M coupling functions are investigated to try and better understand the balance between energy input and storm size, however this will be the topic of our future studies which should include in situ ring current particle measurements, auroral imagery and radar measurements to better quantify this energy balance and develop our understanding of the reasoning behind this new trend.

[69] **Acknowledgments.** The authors would like to thank all those involved in this study as well as the data providers, J. H. King and N. Papatashvilli at AdnetSystems, NASA GSFC, and CDAweb, for providing all of the geomagnetic indices and ACE OMNI data. Sunspot number was provided by SIDC-team, World Data Center for the Sunspot Index, Royal Observatory of Belgium, Monthly Report on the International Sunspot Number, online catalog of the sunspot index, 1997–2008, at http://www.sidc.be/sunspot-data/.

[70] Philippa Browning thanks the reviewers for their assistance in evaluating paper 2011JA016463.

References

Akasofu, S.-I., S. Chapman, and D. Venkatesan (1963), The main phase of great magnetic storms, *J. Geophys. Res.*, *68*(11), 3345–3350, doi:10.1029/JZ068i011p03345.

Burlaga, L. F. (1974), Interplanetary stream interfaces, *J. Geophys. Res.*, *79*(25), 3717–3725, doi:10.1029/JA079i025p03717.

Cowley, S. W. H., and M. Lockwood (1992), Excitation and decay of solar wind-driven flows in the magnetosphere-ionosphere system, *Ann. Geophys.*, *10*, 103–115.

Daglis, I. A., and J. U. Kozyra (2002), Outstanding issues of ring current dynamics, *J. Atmos. Sol. Terr. Phys.*, *64*(2), 253–264, doi:10.1016/S1364-6826(01)00087-6.

Daglis, I. A., R. M. Thorne, W. Baumjohann, and S. Orsini (1999), The terrestrial ring current: Origin, formation, and decay, *Rev. Geophys.*, *37*(4), 407–438, doi:10.1029/1999RG900009.

Denton, M. H., J. E. Borovsky, R. M. Skoug, M. F. Thomsen, B. Lavraud, M. G. Henderson, R. L. McPherron, J. C. Zhang, and M. W. Liemohn (2006), Geomagnetic storms driven by ICME- and CIR-dominated solar wind, *J. Geophys. Res.*, *111*, A07S07, doi:10.1029/2005JA011436.

Echer, E., W. D. Gonzalez, B. T. Tsurutani, and A. L. C. Gonzalez (2008), Interplanetary conditions causing intense geomagnetic storms ($SYM\text{-}H \leq -100$ nT) during solar cycle 23 (1996–2006), *J. Geophys. Res.*, *113*, A05221, doi:10.1029/2007JA012744.

Gonzalez, W. D., J. A. Joselyn, Y. Kamide, H. W. Kroehl, G. Rostoker, B. T. Tsurutani, and V. M. Vasyliunas (1994), What is a geomagnetic storm?, *J. Geophys. Res.*, *99*(A4), 5771–5792, doi:10.1029/93JA02867.

Gonzalez, W. D., B. T. Tsurutani, and A. L. Clúa de Gonzalez (1999), Interplanetary origin of geomagnetic storms, *Space Sci. Rev.*, *88*, 529–562, doi:10.1023/A:1005160129098.

Gopalswamy, N., L. Barbieri, E. W. Cliver, G. Lu, S. P. Plunkett, and R. M. Skoug (2005), Introduction to violent Sun-Earth connection events of October–November 2003, *J. Geophys. Res.*, *110*, A09S00, doi:10.1029/2005JA011268.

Gosling, T. J., and V. J. Pizzo (1999), Formation and evolution of corotating interaction regions and their three dimensional structure, *Space Sci. Rev.*, *89*, 21–52, doi:10.1023/A:1005291711900.

Gosling, J. T., S. J. Bame, D. J. McComas, and J. L. Phillips (1990), Coronal mass ejections and large geomagnetic storms, *Geophys. Res. Lett.*, *17*(7), 901–904, doi:10.1029/GL017i007p00901.

Hamilton, D. C., G. Gloeckler, F. M. Ipavich, W. Stüdemann, B. Wilken, and G. Kremser (1988), Ring current development during the great geomagnetic storm of February 1986, *J. Geophys. Res.*, *93*(A12), 14,343–14,355, doi:10.1029/JA093iA12p14343.

Jordanova, V. K., R. M. Thorne, C. J. Farrugia, Y. Dotan, J. F. Fennell, M. F. Thomsen, G. D. Reeves, and D. J. McComas (2001), Ring current dynamics during the 13–18 July 2000 storm period, *Sol. Phys.*, *204*, 361–375, doi:10.1023/A:1014241527043.

Kamide, Y., N. Yokoyama, W. Gonzalez, B. T. Tsurutani, I. A. Daglis, A. Brekke, and S. Masuda (1998), Two-step development of geomagnetic storms, *J. Geophys. Res.*, *103*(A4), 6917–6921, doi:10.1029/97JA03337.

Klein, L. W., and L. F. Burlaga (1982), Interplanetary magnetic clouds at 1 AU, *J. Geophys. Res.*, *87*(A2), 613–624, doi:10.1029/JA087iA02p00613.

Kokubun, S. (1972), Relationship of interplanetary magnetic field structure with development of substorm and storm main phase, *Planet. Space Sci.*, *20*(7), 1033–1049, doi:10.1016/0032-0633(72)90214-0.

Kozyra, J. U., V. K. Jordanova, J. E. Borovsky, M. F. Thomsen, D. J. Knipp, D. S. Evans, D. J. McComas, and T. E. Cayton (1998), Effects of a high-density plasma sheet on ring current development during the November 2–6, 1993, magnetic storm, *J. Geophys. Res.*, *103*(A11), 26,285–26,305, doi:10.1029/98JA01964.

Liemohn, M. W., and A. A. Chan (2007), Unraveling the causes of radiation belt enhancements, *Eos Trans. AGU*, *88*(42), 425–426, doi:10.1029/2007EO420001.

Liemohn, M. W., J. U. Kozyra, V. K. Jordanova, G. V. Khazanov, M. F. Thomsen, and T. E. Cayton (1999), Analysis of early phase ring current recovery mechanisms during geomagnetic storms, *Geophys. Res. Lett.*, *26*(18), 2845–2848, doi:10.1029/1999GL900611.

Livingston, W., and M. Penn (2009), Are sunspots different during this solar minimum?, *Eos Trans. AGU*, *90*(30), 257–258, doi:10.1029/2009EO300001.

Milan, S. E., J. Hutchinson, P. D. Boakes, and B. Hubert (2009), Influences on the radius of the auroral oval, *Ann. Geophys.*, *27*, 2913–2924, doi:10.5194/angeo-27-2913-2009.

Neugebauer, M., and R. Goldstein (1997), Particle and field signatures of coronal mass ejections in the solar wind, in *Coronal Mass Ejections*, *Geophysical Monograph Ser.*, vol. 99, edited by N. Crooker, J. A. Joselyn, and J. Feynman, pp. 245–251, AGU, Washington, D. C.

Reeves, G. D., K. L. McAdams, R. H. W. Friedel, and T. P. O'Brien (2003), Acceleration and loss of relativistic electrons during geomagnetic storms, *Geophys. Res. Lett.*, *30*(10), 1529, doi:10.1029/2002GL016513.

Richardson, I. G., and J. Zhang (2008), Multiple-step geomagnetic storms and their interplanetary drivers, *Geophys. Res. Lett.*, *35*, L06S07, doi:10.1029/2007GL032025.

Taylor, J. R., M. Lester, and T. K. Yeoman (1994), A superposed epoch analysis of geomagnetic storms, *Ann. Geophys.*, *12*(7), 612–624, doi:10.1007/s00585-994-0612-4.

Tsurutani, B. T., W. D. Gonzalez, A. L. C. Gonzalez, F. Tang, J. K. Arballo, and M. Okada (1995), Interplanetary origin of geomagnetic activity in the declining phase of the solar cycle, *J. Geophys. Res.*, *100*(A11), 21,717–21,733, doi:10.1029/95JA01476.

Wanliss, J. A., and K. M. Showalter (2006), High-resolution global storm index: *Dst* verses *SYM-H*, *J. Geophys. Res.*, *111*, A02202, doi:10.1029/2005JA011034.

Yokoyama, N., and Y. Kamide (1997), Statistical nature of geomagnetic storms, *J. Geophys. Res.*, *102*(A7), 14,215–14,222, doi:10.1029/97JA00903.

Zhang, J., M. W. Liemohn, J. U. Kozyra, M. F. Thomsen, H. A. Elliott, and J. M. Weygand (2006), A statistical comparison of solar wind sources of moderate and intense geomagnetic storms at solar minimum and maximum, *J. Geophys. Res.*, *111*, A01104, doi:10.1029/2005JA011065.

J. A. Hutchinson, S. E. Milan, and D. M. Wright, Department of Physics and Astronomy, University of Leicester, University Road, Leicester, LE1 7RH, U. K. (jh251@ion.le.ac.uk)